

Unveiling the chaotic structure in phase space of molecular systems using Lagrangian descriptors

F. Revuelta,^{1,2,*} R. M. Benito,^{1,†} and F. Borondo^{2,3,‡}

¹*Grupo de Sistemas Complejos, Escuela Técnica Superior de Ingeniería Agronómica, Alimentaria y de Biosistemas, Universidad Politécnica de Madrid, Avda. Puerta de Hierro 2-4, 28040 Madrid, Spain*

²*Instituto de Ciencias Matemáticas (ICMAT), Cantoblanco, 28049 Madrid, Spain*

³*Departamento de Química, Universidad Autónoma de Madrid, Cantoblanco, 28049 Madrid, Spain*



(Received 13 August 2018; revised manuscript received 25 January 2019; published 27 March 2019)

We explore here the feasibility of using the recently introduced Lagrangian descriptors [A. M. Mancho *et al.*, *Commun. Nonlinear Sci. Numer. Simul.* **18**, 3530 (2013)] to unveil the usually rich dynamics taking place in the vibrations of molecular systems, especially if they are floppy. The principal novelty of our work is the inclusion of p norms in the definition of the descriptors in this kind of system, which greatly enhances their power to discern among the different structures existing in the phase space. As an illustration we use the LiCN molecule described by realistic potentials in two and three dimensions, which exhibits chaotic motion within a mixed phase space in the isomerization between the two wells corresponding to the linear isomer stable configurations, LiNC and LiCN. In particular, we pay special attention to the manifolds emerging from the unstable fixed point between the corresponding isomer wells, and also to the marginally stable structures around a parabolic point existing near the LiNC well.

DOI: [10.1103/PhysRevE.99.032221](https://doi.org/10.1103/PhysRevE.99.032221)

I. INTRODUCTION

The rich dynamics usually exhibited by generic nonlinear systems is strongly influenced by the structures existing in their phase spaces [1]. Some of them, like invariant tori, confine trajectories in particular specific regions, where the motion is regular. Contrary, other trajectories have a more complex, yet chaotic, behavior, thus being much more complicated to compute and characterize, as Poincaré early discovered [2]. Still, their behavior is strongly influenced by invariant manifolds, which attract or repel motion toward or apart from different regions in phase space.

The phase-space structure of conservative Hamiltonian systems with two degrees of freedom (2-dof) can be very well characterized using Poincaré surface of sections (PSOS). In these systems, the phase space is four dimensional, and the motion is always confined in the three-dimensional energy shell. If the value of one of the coordinates and the conjugate momentum are measured simultaneously on a certain plane, i.e., that defining the PSOS, the dynamics is then easily visualized and characterized. PSOS can then be used to identify invariant tori (rendering curves in the PSOS picture), which always correspond to regular motion, and those regions where chaotic motion takes place, which is shown as a dense sea of points, typically with no recognizable pattern at all. These chaotic regions emerge when invariant tori break down, as the celebrated Kolmogorov-Arnold-Moser (KAM) and the Poincaré-Birkhoff theorems [1] dictate.

Nevertheless, the chaotic regions of phase space are not free from organization and hierarchy. Indeed, underlying

structures exist, such as unstable periodic orbits (POs) and their associated invariant manifolds. In general, they present an infinite number of intersections, the so-called *homoclinic tangle* first described by Poincaré, whose infinite crossings and recrossings are responsible for all the complexity of the chaotic dynamics. Actually, these tangles, which can be either homoclinic (intersections of the invariant manifolds associated with a single PO) or heteroclinic (intersections associated with the invariant manifolds of different POs) are cornerstones for the dynamics of nonlinear systems. Thus, their identification is key for a correct dynamical characterization of this kind of system.

Unfortunately, PSOSs are difficult to visualize in systems with more than 2-dof because of their higher dimension. For example, the Poincaré map in a system with 3-dof is four dimensional. As a consequence, new visualization tools were developed for this purpose (see, for example, Refs. [3–7]). Also, other indicators of chaos and regular motion, measuring the stability of trajectories, were defined and used. Lyapunov exponents [8], measuring the stability of trajectories, are one of them. However, they are often difficult to compute, since their convergence is, in general, only achieved after an extremely long propagation in time [8]. Other short-time alternatives, such as fast Lyapunov indicators (FLI) [9,10] and their variants [11], circumvent the previous problem, being then much better suited for the task. Also, the small alignment index (SALI) [12,13], and the mean exponential growth factor of nearby orbits [14] are also efficient alternatives, much less demanding computationally than the Lyapunov exponents.

Very recently, another powerful indicator of chaos, known as *Lagrangian descriptors (LDs)*, has been introduced. These descriptors focus on the phase-space structures that are embedded in the chaotic regions of phase space. They were first introduced by Madrid and Mancho [15] under the name of

*fabio.revuelta@upm.es

†rosamaria.benito@upm.es

‡f.borondo@uam.es

M function for the characterization of aperiodic flows. Later, they were applied to the study of maps [16–18], and stochastic systems [19]. Moreover, LDs have also been successfully implemented [20] within the so-called geometric transition state theory [21,22] for the identification of recrossing-free dividing surfaces [23–27], thus helping in the computation of chemical reaction rates. Also, LDs have been used in the identification of reactive islands that account for nonstatistical behavior in chemical reactions [28].

In this paper, we apply LDs to study the dynamics of the LiCN molecule with 2- and 3-dof, an isomerizing system with a very floppy motion in the angular coordinate, which explores wide regions of the potential energy surface. This implies important couplings with the other dofs and then a rich dynamical behavior. As a result, chaos sets in at very low values of the excitation energy. Actually, the LiCN molecule can be taken as a benchmark for the study of classical and quantum chaos, and their correspondence [13,29–31], for two reasons. First, this system has a mixed phase space, which combines regular and irregular motion at the same energy, a characteristic of generic chaotic systems. Second, the system has in configuration space two wells separated by a modest energetic barrier; thus, it can be used as an ideal model to test methods designed to study prototypical double wells with 1-dof, extending them to higher dimensions in a more realistic situation.

In this paper, we demonstrate the ability of LDs to efficiently and adequately describe the underlying relevant structures in the phase space of our realistic system, and we show how LDs constitute an excellent alternative to that offered by (composite) PSOSs, especially when the latter is difficult to visualize. Furthermore, we show that LDs are able to unveil the structures existing in the chaotic regions of phase space, which leave no obvious imprint in the Poincaré maps. Likewise, we demonstrate that LDs exhibit a pattern that totally mimics the tangles associated with homoclinic oscillations, which originates the complex motion in nonlinear systems. The computation of LDs also unveils the existence of other structures, such as chain of islands or an interesting cantorus related to a parabolic point [1] that appears in a saddle-node bifurcation [32–34]. Moreover, other computational aspects associated with LDs are explored in this paper. In particular, we ascertain the improvement in the performance of the LD that it is obtained when *p* norms, instead of the standard norm, are used in their definition. Also, we study the effects of the integration time used in the calculations.

This paper is organized as follows. First, we describe in Sec. II the molecular system under study. Second, we discuss in Sec. III some results about its reduced dynamics for two energies relevant to our study using PSOS in a reduced two-dimensional Hamiltonian. Third, we introduce in Sec. IV the basics of the LD, and discuss some alternatives on their computation. Fourth, we present in Sec. V the results of our study along with the corresponding discussion. Fifth, we conclude the paper in Sec. VI with a brief summary and outlook.

II. MODEL

The system under study is the floppy isomerizing $\text{LiNC} \rightleftharpoons \text{LiCN}$ system. Using Jacobi coordinates, the vibrational

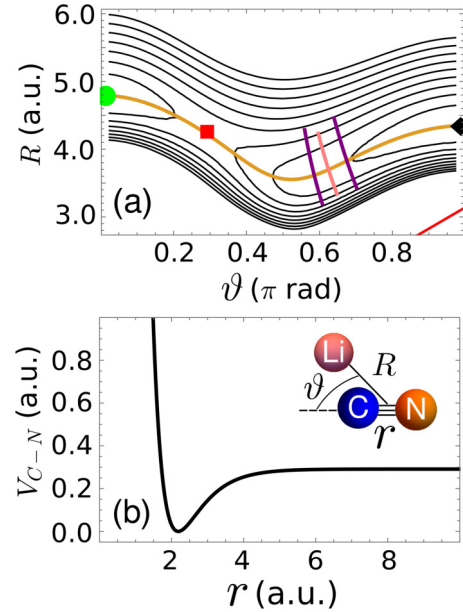


FIG. 1. Potential energy surface for the LiCN molecule, $V(R, \vartheta, r) = V_{\text{Li-CN}}(R, \vartheta) + V_{\text{C-N}}(r)$. (a) Contour plot for $V_{\text{Li-CN}}(R, \vartheta)$. The existence of two minima, corresponding to the stable collinear isomers: Li-CN at $\vartheta = 0$ rad (green circle), and CN-Li at $\vartheta = \pi$ rad (black diamond), is seen. These two isomers are connected by the minimum energy path (brown line), which crosses a modest barrier (red square). Three relevant periodic orbits are also shown as almost vertical lines. (b) Morse function (3) for the C-N dimer potential, $V_{\text{C-N}}(r)$. The definition of the Jacobi coordinates, (R, ϑ, r) , used in our calculations is shown in the inset for the configuration of the isomerization reaction, $\text{LiNC} \rightleftharpoons \text{LiCN}$, transition state formed at the barrier top localized at $\vartheta = 0.292 \pi$ rad.

($J = 0$) Hamiltonian is given by

$$\mathcal{H} = \frac{p_R^2}{2\mu_1} + \frac{p_\vartheta^2}{2I_\vartheta(R, r)} + \frac{p_r^2}{2\mu_r} + V(R, \vartheta, r), \quad (1)$$

where R , ϑ , and r describe the Li-CN stretching, the Li-C-N bending, and the C-N stretching motions, respectively, as shown schematically in the inset to Fig. 1(b). The corresponding reduced masses are $\mu_1 = m_{\text{Li}}m_{\text{CN}}/m_{\text{LiCN}}$ and $\mu_2 = m_{\text{C}}m_{\text{N}}/m_{\text{CN}}$, respectively, with $m_{\text{LiCN}} = m_{\text{Li}} + m_{\text{C}} + m_{\text{N}}$ and $m_{\text{CN}} = m_{\text{C}} + m_{\text{N}}$. $I_\vartheta(R, r) = [1/(\mu_r R^2) + 1/(\mu_r r^2)]^{-1}$ is the reduced moment of inertia associated with the ϑ -dof. Notice that while the reduced masses μ_1 and μ_2 , respectively associated with R and r , are constant, the reduced moment of inertia I_ϑ depends on the value of the distances R and r . As a consequence, the corresponding kinetic term introduces a coupling between the previous coordinates and the angular dof, ϑ . Further details on this coupling between the different dofs and on the definition of Jacobi coordinates can be found, for example, in the Ref. [35].

The potential energy surface (PES) is split into two parts

$$V(R, \vartheta, r) = V_{\text{Li-CN}}(R, \vartheta) + V_{\text{C-N}}(r), \quad (2)$$

being $V_{\text{Li-CN}}(R, \vartheta)$, the potential associated with the molecule when the distance C-N is kept fixed at its equilibrium value, $r_e = 2.186$ a.u. [36]. This term is mostly responsible for the

coupling between the R and ϑ dofs. The second term, $V_{C-N}(r)$, corresponds to the potential interaction for the C-N stretching, and it is described by a Morse function

$$V_{C-N}(r) = D[1 - e^{-\beta(r-r_e)}]^2, \quad (3)$$

with $D = 0.29135$ a.u., and $\beta = 1.4988$ a.u. These two contributions are shown in Figs. 1(a) and 1(b), respectively.

As can be seen, the LiNC-LiCN system presents two minima, corresponding to the two stable collinear isomers: Li-CN at $\vartheta = 0$ rad and $r = r_e$, and CN-Li at $\vartheta = \pi$ rad and $r = r_e$, respectively, being the latter the most stable one. These two isomers are connected by the minimum energy path, $R_e(\vartheta)$ [shown as a brown line in Fig. 1(a)], which crosses a modest barrier (also marked with a red square in the figure).

III. DYNAMICS

The dynamics of the LiCN molecule is very floppy, and then chaos sets in at very low values of the excitation energy. Moreover, the C-N vibrational frequency is very high and then, to a good approximation, the r motion can be considered decoupled from the rest of the motions in the molecule. Accordingly, the system can be adequately described by a 2-dof model corresponding to keeping r frozen at its equilibrium value, which is described by the following vibrational ($J = 0$) Hamiltonian:

$$\mathcal{H}_2 = \frac{P_R^2}{2\mu_R} + \frac{P_\vartheta^2}{2I_\vartheta(R, r_e)} + V_{\text{Li-CN}}(R, \vartheta). \quad (4)$$

In this case, the dynamics can be followed by means of composite PSOSs, using the minimum energy path as the sectioning plane, i.e., $R = R_e(\vartheta)$ and, for example, $\psi > 0$. Moreover, to make this PSOS an area preserving map, the following canonical transformation must be used [29]:

$$\rho = R - R_e(\vartheta), \quad (5a)$$

$$P_\rho = P_R, \quad (5b)$$

$$\psi = \vartheta, \quad (5c)$$

$$P_\psi = P_\vartheta - \left(\frac{dR_e}{d\vartheta} \right)_{\vartheta=\psi} P_R. \quad (5d)$$

Finally, taking into account the dynamical symmetry of the problem, the computed plot can be simplified by performing the following folding procedure:

$$\psi \rightarrow \psi - \left\lfloor \frac{\psi}{2\pi} \right\rfloor 2\pi, \quad \text{if } |\psi| > 2\pi, \quad (6a)$$

$$\psi \rightarrow 2\pi + \psi, \quad \text{if } \psi < 0, \quad (6b)$$

$$\psi \rightarrow 2\pi - \psi \text{ and } P_\psi \rightarrow -P_\psi, \quad \text{if } \psi > \pi. \quad (6c)$$

where $\lfloor \dots \rfloor$ is the floor function.

Some results for moderate values of the excitation energy are shown in Fig. 2. As can be seen, for the lowest chosen value of the energy [panel (a)] all motions take place around the most stable Li-NC isomer, and they are completely regular. Accordingly, the dynamics is confined into invariant tori, which render closed curves in the PSOS that foliate the available phase space in an onionlike fashion. Moreover, the chains of islands corresponding to the resonances $(n_R : n_\vartheta) = (1 : 6)$,

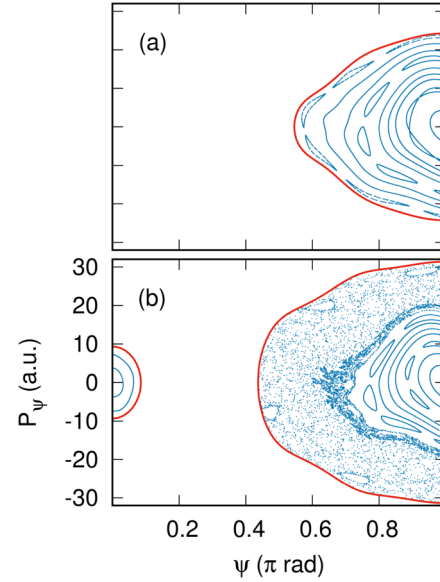


FIG. 2. LiCN composite Poincaré surface of sections (ψ, P_ψ) , taking $\rho = 0$ and $\dot{\psi} > 0$ [see definitions in Eqs. (5)] for the 2-dof model of LiCN corresponding to Eq. (4) for $E = 1500 \text{ cm}^{-1}$ (a), and $E = 2500 \text{ cm}^{-1}$ (b).

(1 : 8), and (1 : 10) are readily observed. The fate of these structures is dictated by the Poincaré-Birkhoff theorem [1].

As the energy increases to $E = 2500 \text{ cm}^{-1}$ [panel (b)] some of the previously observed tori are destroyed, i.e., the one corresponding to the (1 : 10) resonance, turning into a conspicuous sea of points. As a consequence an ample region of chaos representing irregular vibrational motion is seen. Embedded in it, and next to the border of the available phase space the chain of islands of stability corresponding to a new (1 : 8) resonance is also apparent. It has different characteristics from the resonance (1 : 8) observed in Fig. 2(a), as discussed in Ref. [30]. Notice also that the stable chain of islands (1 : 6) and the old (1 : 8) have survived. More interesting is the accumulation of points that is observed just outside the border of the regular region. This is indicative of the existence of a cantorus, which was studied in detail by some of us in the past [32–34], and will play a relevant role in the discussion of the LD results presented in the next section. Cantori constitute partial barriers for the flux of trajectories across [37], this explaining the accumulation of points in the area between the cantorus and the last unbroken invariant tori [located closer to the center $(\psi, P_\psi) = (\pi \text{ rad}, 0 \text{ a.u.})$]. Notice also the appearance, at this value of the energy, of an area of regularity in a small neighborhood of the Li-CN isomer, i.e., around $\psi = 0$ rad, which is now energetically accessible.

IV. LAGRANGIAN DESCRIPTORS

In this section, we describe the use of LDs to study the phase space of the isomerizing LiNC-LiCN molecular system, which is the main goal of the present work. Essentially, LDs measure the arc length of a trajectory launched at a specific point of phase space. The dynamical character and behavior of the trajectory, determined by the corresponding

Hamiltonian flow, will leave an imprint on the LD, which can in this way be easily ascertained. Actually, LDs present an abrupt change at the boundaries of regions comprising trajectories with qualitatively different time evolution, which manifests as a discontinuity in the derivative transverse to that boundary [38]. As will be shown in Sec. V below, the previous singularity appears, for example, along the invariant manifolds of hyperbolic trajectories, irrespective of them being periodic, aperiodic, or chaotic. The heuristic argument would still apply to our case, indicating that at the boundaries of regions comprising trajectories with qualitatively different time evolution the accumulated value of the chosen positive quantity will change abruptly.

A. Standard definition of the Lagrangian descriptors

Following early work by Haller on strain tensors [39], the first definition of LDs was introduced by Madrid and Mancho [15] as

$$M_s(\mathbf{z}_0, \tau) = \int_{-\tau}^{\tau} \sqrt{\sum_{i=1}^n \dot{z}_i^2(t)} dt, \quad (7)$$

that is, the Euclidean norm of the flow $\dot{\mathbf{z}}(t) = \mathbf{f}(\mathbf{z}, t)$, with the initial condition $\mathbf{z}_0 = (R_0, \vartheta_0, r_0, P_{R,0}, P_{\vartheta,0}, P_{r,0})$ in our case, and integrated over the time interval $[-\tau, \tau]$. Hereafter, we will refer to this definition of LD as the *standard* one.

Notice that the time evolution involved in Eq. (7) is performed forward and backward in order to account for the stable and unstable manifolds of hyperbolic orbits all at once. Recall that the unstable (stable) invariant manifold determines the dynamics forward (backward) in time, and then its imprint in the LD is (almost) solely manifested by performing the corresponding time evolution. Let us remark here that the computation of the LD using Eq. (7) [and Eq. (8) below] requires solely the propagation (forward and backward in time) of the initial condition under study. On the contrary, for the calculation of SALI one must also integrate two neighboring trajectories [12,13], and for FLI (in an n -dimensional phase space) the integration of n neighboring trajectories [10] is required.

Obviously, the integration time τ plays an important role in the definition and actual computation of LDs. Let us next discuss the influence of this parameter in LDs, and how the best suited value of it can be selected in our calculation.

In Fig. 3 we show some results for the 2-dof model of LiCN [see Eq. (4)] for $E = 2500 \text{ cm}^{-1}$, the same one used in Fig. 1(b). A fine grid of initial conditions on the PSOS is chosen, and then the corresponding LD computed using Eq. (7) for different values of the integration time τ . The obtained numerical results are represented on the chosen PSOS point using a color code that alternates cold and warm colors in order to enhance the difference between adjacent trajectories. The reason for this is that the most important issue in the LD, as defined in Eq. (8), is to consider the changes in the value (color) of the LD. [16–18,38].

As can be seen in Fig. 3(a), the LD is a smooth function for the shortest integration times considered ($\tau = 10^3 \text{ a.u.}$); then, no invariant structure is resolved. This is not an unexpected result since the stability exponent of a typical unstable

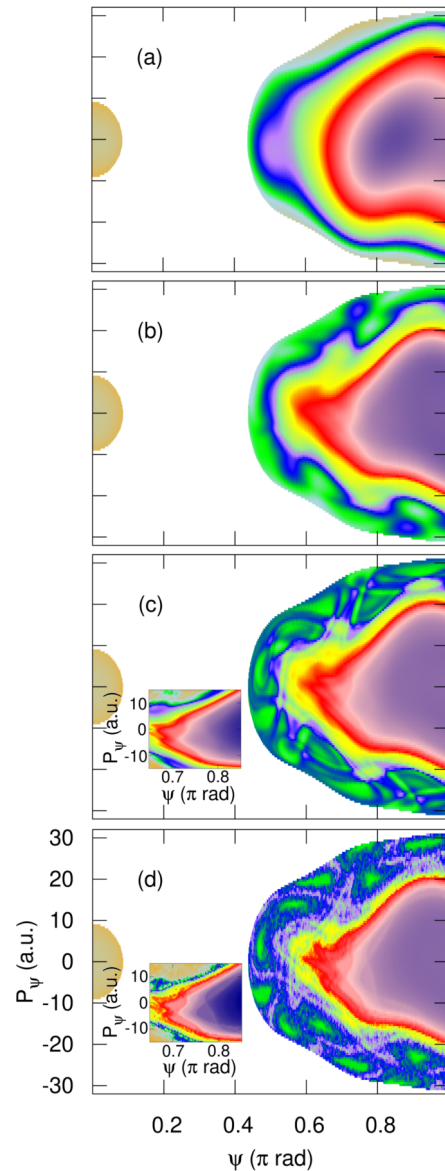


FIG. 3. Lagrangian descriptors for the LiCN 2-dof model (4) for $E = 2500 \text{ cm}^{-1}$ [the same one used in Fig. 2(b)] using the standard definition (7) for different values of τ : (a) 10^3 a.u. , (b) 10^4 a.u. , (c) $2 \times 10^4 \text{ a.u.}$, and (d) 10^5 a.u. , respectively.

periodic orbit at this energy is of order $\lambda \sim O(10^{-4})$, and then $\lambda \tau \sim O(10^{-1})$, a value which is too small to distinguish the hyperbolic behavior of two neighboring chaotic trajectories. It is only when the integration time is sufficiently large that the dynamics in different regions in phase space leave clearly distinguished imprints on the LD plots, becoming then visible. Notice, for example, that the LD plot shown in Fig. 3(b), which corresponds to $\tau = 10^4 \text{ a.u.}$, has a shape that very much resembles that of the composite PSOS of Fig. 2(b). This value of τ is still neither long enough to identify the invariant structures in the chaotic regions of phase space, nor to identify the chains of islands of stability.

Furthermore, when τ is further increased to $2 \times 10^4 \text{ a.u.}$ the chaotic region of the PSOS in Fig. 2(b), which only consists of a dense sea of points with no apparent or identifiable

pattern, exhibits an involved shape in the LD plot shown in Fig. 3(c), where abrupt changes in the coloring mark the existence of invariant manifolds.

However, when much longer integration times are used, a more detailed description of the local properties of the invariant manifolds is included in the computed LD, and then they no longer appear as continuous lines in the LD plots but as blurry ones. This is the case seen in Fig. 3(d), where $\tau = 10^5$ a.u. Let us remark that this value of the integration time is only ~ 50 times larger than that of the periods of the POs shown in Fig. 1. Nevertheless, this longer integration time is useful to resolve the chains of islands that are embedded in the more regular region of phase space that exists in the LiNC well ($\psi = \pi$ rad) located inside the cantorus that is seen as a dense set of points in Fig. 2(b). The two insets presented in Figs. 3(c) and 3(d) show enlarged views of these regions. As seen, the chain of islands associated with the resonance (1 : 8), which is clearly visible in the PSOS of Fig. 2(b), becomes also visible in the LD computed for the longest integration time, but not for the previous (smaller) considered values of τ .

As a result, we can conclude that τ is a crucial parameter, that should be heuristically chosen to get meaningful LD results. In our case a value of $\tau = 2 \times 10^4$ a.u. seems adequate for our purposes. Unfortunately, there is no explicit way to predict an adequate value of it, and then only a trial-and-error procedure can be performed to set its value.

B. Lagrangian descriptors defined using p norms

Although definition (7) has been demonstrated to be extremely fruitful since its inception, very recently Mancho *et al.* [38,40] have elaborated an alternative definition for the LD, which allows the identification of phase-space structures using shorter computation times. This new and improved definition of the LD characterizes the flow using a p norm in the following way:

$$M_p(\mathbf{z}_0, \tau) = \int_{-\tau}^{\tau} \sum_{i=1}^n |\dot{z}_i|^p dt, \quad (8)$$

with $p \leq 1$. Notice that for $p = 1$ the p norm appearing in Eq. (8) is the so-called *taxicab* or *Manhattan norm*, giving in two dimensions the distance corresponding to moving in a rectangular grid to the final point. Unfortunately, to the best of our knowledge, no such straightforward interpretation of the p norm for other smaller values of p exists.

Let us now demonstrate the improvement obtained when using p norms in the definition of the LD [see Eq. (8)], which provides a more efficient alternative to study the structure of phase space, especially when the dynamics is chaotic. For this purpose, we show in Fig. 4 the LD computed for the (approximately) optimized value of the integration time $\tau = 2 \times 10^4$ a.u., and different values of p . Notice how in all cases, the computed LD reveals some structures in the chaotic region that can be easily identified in an unambiguous fashion, this being especially true in panels (a) and (b). When closely examined, they are seen to correspond to the invariant manifolds defining the tangle that emanates from the unstable points of the different chain of islands, mainly those corresponding to the outer (1 : 8) resonance existing in this region of the LiNC

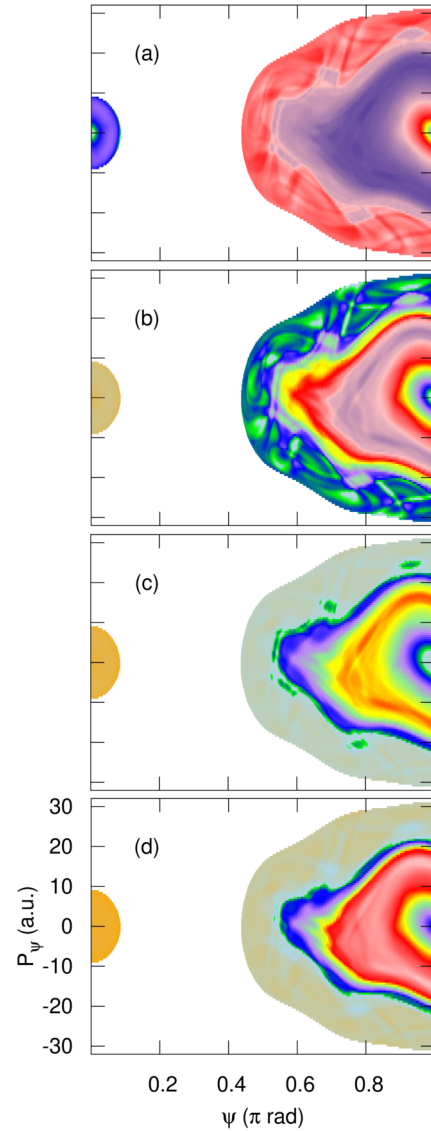


FIG. 4. Same as Fig. 3 computed using different p norms, as defined in Eq. (8): (a) $p = 0.1$, (b) $p = 0.4$, (c) $p = 0.6$, and (d) $p = 1$. An integration time $\tau = 2 \times 10^4$ a.u. has been used in all cases.

phase space, which was discussed in connection with the results in Fig. 2(b). The imprint of these structures in the LD is much weaker in panels (c) and (d), where the $p = 0.6$ or $p = 1.0$ norms are used instead in the definition of the LD. Contrary to what happened for the standard LD, the chains of islands that emerge in the frontier between regular and irregular motion are here more clearly seen due to the use of p norms.

Let us finally sum up this section by pointing out that the computation time for the LD has the same effect for both standard and p -norm definitions: namely, if it is too low, the LDs show up as a smooth function, while too high values of the integration time render LD plots with too much information, and then the existing structures cannot be identified. Moreover, our results show that a value of $p = 0.4$, which is very close to that of ~ 0.5 suggested by Mancho *et al.* [38,40], seems to be best suited to identify the invariant manifolds that partition the chaotic phase space in our case, and accordingly

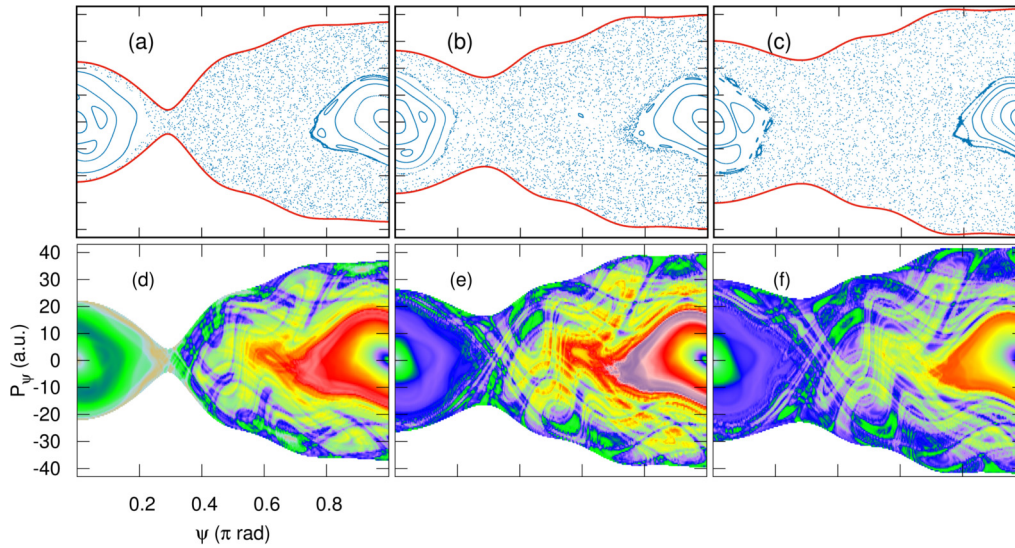


FIG. 5. Composite Poincaré surface of sections (a)–(c) and Lagrangian descriptors computed with $p = 0.4$ and $\tau = 2 \times 10^4$ a.u. (d)–(f) for the 2-dof model of the LiCN molecule corresponding to Eq. (4), for different values of the vibrational energy: $E = 3500 \text{ cm}^{-1}$ [(a) and (d)], $E = 4000 \text{ cm}^{-1}$ [(b) and (e)], and $E = 4500 \text{ cm}^{-1}$ [(c) and (f)].

all calculations presented hereafter will be performed using this specific p norm.

V. RESULTS AND DISCUSSION

In this section we report the results of our LD calculation and present the corresponding discussion. All LDs discussed here have been computed using Eq. (8) with $p = 0.4$ and $\tau = 2 \times 10^4$ a.u.

The results are presented divided into two parts. First, we report in Sec. V A the phase-space analysis for the 2-dof model of the LiCN molecule corresponding to Eq. (4), where the C-N distance is kept fixed at its equilibrium value, paying special attention to the neighborhood of the marginally stable structures associated with the POs plotted in pink and purple in Fig. 1(a). Second, Sec. V B is devoted to the case where the full dynamics is taken into account, i.e., when the system is studied with the 3-dof realistic model of Eqs. (1)–(3).

A. Two-degrees-of-freedom model

Here we extend our study of the 2-dof model for LiCN presented in Sec. III, by considering vibrational excitation energies above that of the saddle point [red square in Fig. 1(a)] existing in $V_{\text{Li-CN}}(R, \vartheta)$ in Eq. (2).

In Figs. 5(a)–5(c) we show the composite PSOS for this model corresponding to $E = 3500, 4000,$ and 4500 cm^{-1} . Notice that all these energies allow the “rotation” of the Li atom around the CN fragment, and thus the isomerization process $\text{LiNC} \rightleftharpoons \text{LiCN}$. Here, the energy shell is formed by a single connected volume, and not by two disconnected regions as in the cases shown in Figs. 2–4. As expected, the degree of chaoticity of the system has increased with the energy, as can be inferred by visual inspection of the plots in these three panels. In the corresponding chaotic areas, irregular motions exist, which allows the transport from different (distant) regions.

However, despite its numerical relevance, the PSOS offer no clue of the (rich) underlying structure in these chaotic regions, providing only detailed information of the regular motion around the isomers. The situation is totally different in Figs. 5(d)–5(f), where the corresponding results for the p -norm computed LDs are displayed. In all of them, the tangles existing in the chaotic regions, which in our case are mainly due to the homoclinic intersections of the one-dimensional stable and unstable invariant manifolds emanating from the unstable fixed point corresponding to the PO at the saddle of the PES [see Fig. 1(a)], are clearly visible. In fact, the imprint of these manifolds, which are able to fully partition, in an exact way, the phase space in the chaotic regions [1,41], is so clear, that the LD plots can be used to compute them [20]. Notice that although this calculation can be carried out numerically using standard nonlinear techniques, this task gets progressively more complicated as the dimensionality of the problem raises, and then using LD as a first approximation alleviates the computational burden, since it only requires solving the system equations of motion and performing the integral in Eqs. (7) or (8). Moreover, this way of proceeding has the additional advantage of being easy to understand, this opening a convenient door to the novice into this field.

Let us finish this section by discussing another relevant point of our work, which is the ability of LDs to unveil the structures in the neighborhood of a (marginally stable) parabolic point in phase space, where the dynamics is non-hyperbolic. To the best of our knowledge, to date, there is no rigorous proof of the existence of discontinuities in the LD in the vicinity of such points, contrary to what happens for the regular unstable fixed-point case [16–18].

One such parabolic region exists in the dynamics of our 2-dof model for LiCN. As discussed in detail in Refs. [32–34,42], this and associated structures are due to the occurrence of a saddle-node bifurcation at $E_{\text{bif}} = 3440.6 \text{ cm}^{-1}$, where a degenerate pair of marginally stable

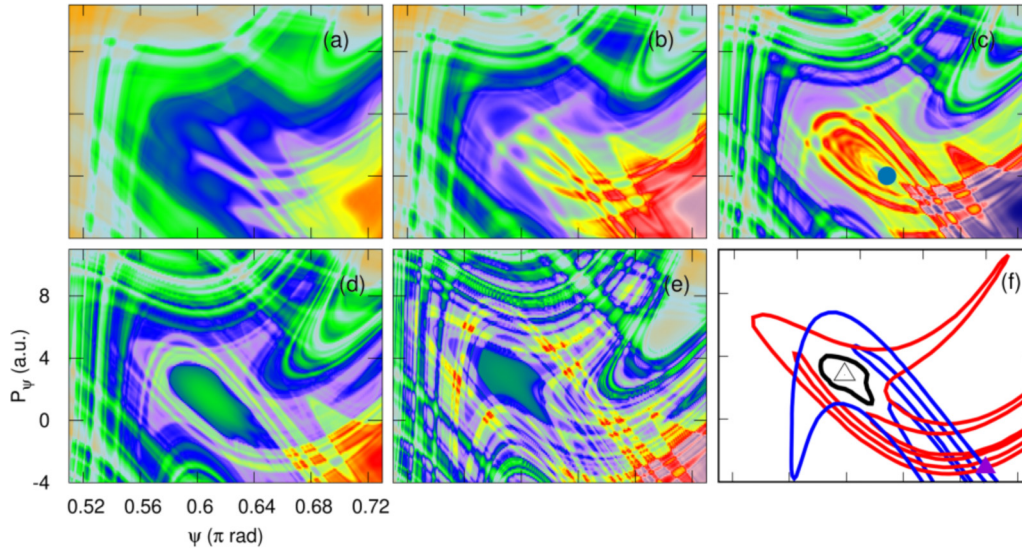


FIG. 6. Lagrangian descriptors computed with $p = 0.4$ and $\tau = 2 \times 10^4$ a.u. (a)–(e) for the 2-dof model of the LiCN molecule corresponding to Eq. (4) for different values of the vibrational energy below, at, and above the energy, E_{bif} , of the saddle-node bifurcation discussed in the text: $E = 3000 \text{ cm}^{-1}$ (a), $E = 3200 \text{ cm}^{-1}$ (b), $E = E_{\text{bif}} = 3440.6 \text{ cm}^{-1}$ (c) where the blue filled circle indicates the position of the parabolic point, $E = 3700 \text{ cm}^{-1}$ (d), and $E = 4163.3 \text{ cm}^{-1}$ (e). The composite Poincaré surface of section (adapted from Ref. [33]) corresponding to (e), showing the phase-space structures associated with the bifurcation, is also presented, for comparison, in (f). In it, the fixed points corresponding to the stable and unstable periodic orbits [see purple lines in Fig. 1(a)] are indicated with an open and a full purple triangle, respectively. An invariant torus (black solid line) around the former, and the stable (blue line) and unstable (red line) manifolds emanating from the latter are also shown.

POs, drawn in pink in Fig. 1(a), appear *out of the blue*, or more precisely as the result of a series of high-order precursor POs, which already exist below the bifurcation energy, as discussed in detail in Fig. 6 of Ref. [33], where the (1:24) and (1:28) precursors (oscillating around the LiNC isomer) are shown. These two POs later evolve, as energy increases, separating from each other [see purple orbits in Fig. 1(a)], being stable that on the left side and unstable that on the right side of the original one, this giving rise to interesting dynamical properties of this region. Indeed, in these nonhyperbolic regions the existing stable and unstable manifolds intersect at very small angles, or have tangencies which give rise to infinite series of saddle-node bifurcations [33], which mix with the bifurcations of the principal POs (around the LiNC in our case), whose existence is guaranteed by the Weinstein theorem [43]. All this makes the dynamics in this region very complicated, and the proliferation of folds in the precursor POs accumulate in the region where the “future” saddle-node orbit will be born. As indicated before very few of these structures are apparent, if at all, in the PSOS. For example, in Fig. 5(b) only a tiny island of regularity is seen, around $(\psi, P_\psi) \simeq (0.6\pi \text{ rad}, 0 \text{ a.u.})$, while nothing is obvious in panels (a) and (c).

To study the issue in detail, we present in Fig. 6 the results corresponding to p -norm computed LDs at energies below [panels (a) and (b)], at [panel (c)], and above [panels (d) and (e)] that of the bifurcation point $E_{\text{bif}} = 3440.6 \text{ cm}^{-1}$. The position of the parabolic point is indicated with a filled blue circle in panel (c). As can be seen, the colored LDs clearly indicate the existence of a complicated dynamical structure, which changes with the energy. More interesting,

LDs also show that this structure does not appear *out of the blue* at the bifurcation energy, but it also exists below it, being there formed by the manifolds associated with high-order POs oscillating around the Li-NC isomer, and intersecting at small angles. All these results are in agreement with the conclusions of Ref. [33], where complete details were given in the discussions corresponding to its Figs. 6–10. Actually, the similarities existing between the LD structures in Figs. 6(c) and 6(d) and those in Figs. 8(c) and 8(f) of that reference are quite remarkable. Finally, we are also giving, for comparison, in Fig. 6(f), a zoom-in of the portion of the PSOS computed at $E = 4163.3 \text{ cm}^{-1}$ corresponding to Fig. 6(e), where the structure emerging from the parabolic point, i.e., hyperbolic point (filled purple triangle) and associated manifolds enveloping the regularity region around the elliptic point (empty triangle and black KAM tori), appears fully developed. (The reason for choosing this particular value of the energy is that it is equal to that of the 79th vibrational eigenstate of the LiNC-LiCN isomerizing system, which is very much influenced by the above discussed structure [32,33]). In it, we have only included the most relevant elements. The position of the fixed points corresponding to the stable and unstable saddle-node POs [see also POs in purple in Fig. 1(a)], are indicated with an open and a filled purple triangle, respectively. Also, an invariant KAM torus enveloping the island of regularity around the former is plotted in a black solid line, while the remaining lines represent different portions of the stable and unstable manifolds associated with the unstable PO, which have been colored for better visualization. As can be seen, the homoclinic tangle and regular region in this plot are extremely well mimicked by the colored LDs of panel (e).

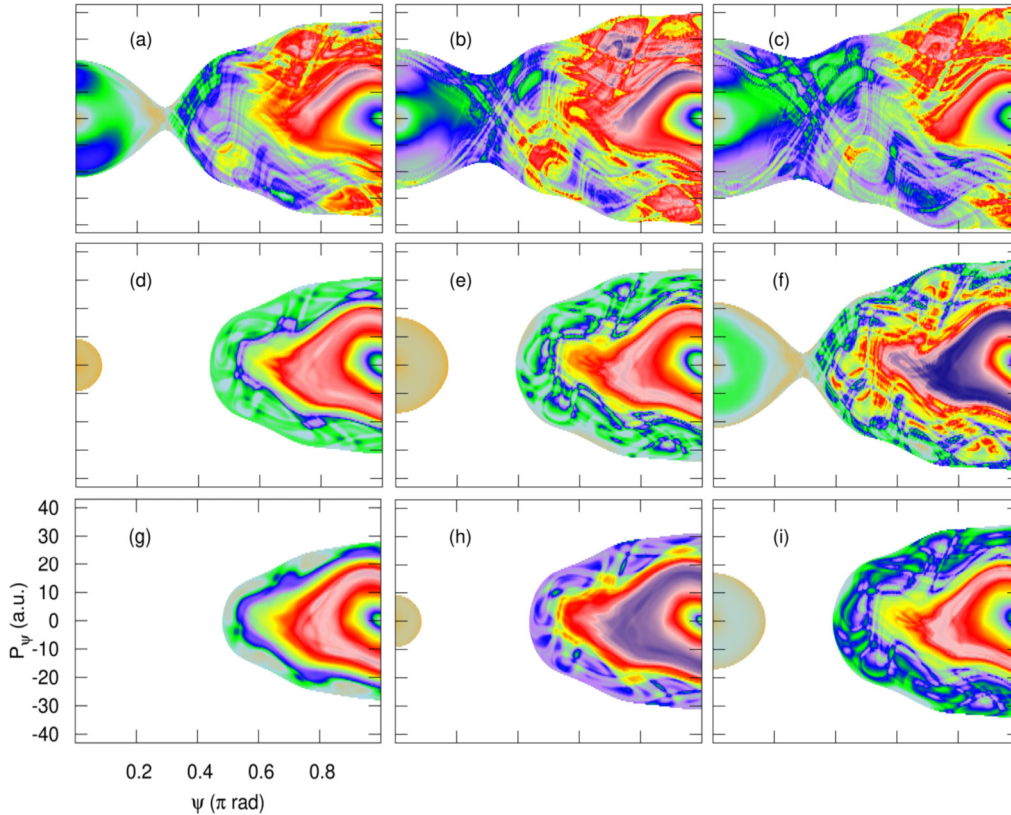


FIG. 7. Lagrangian descriptors computed using $p = 0.4$ and $\tau = 2 \times 10^4$ a.u. for the 3-dof model of the LiCN molecule corresponding to Eq. (1), for different values of the total vibrational energy: $E = 3500 \text{ cm}^{-1}$ (left column), $E = 4000 \text{ cm}^{-1}$ (middle column), and $E = 4500 \text{ cm}^{-1}$ (right column), and different choices of the initial fraction on the CN kinetic energy: $T_{\text{kin}}^{\text{CN}} = 0 \text{ cm}^{-1}$ (top row), $T_{\text{kin}}^{\text{CN}} = 1000 \text{ cm}^{-1}$ (middle row), and $T_{\text{kin}}^{\text{CN}} = 1500 \text{ cm}^{-1}$ (bottom row).

B. Three-degrees-of-freedom model

Let us consider now the p -norm computed LDs for the LiCN molecular vibrations when described with the 3-dof model of Sec. II, which gives full account of the C-N motion. The corresponding phase space will now be six dimensional, and the energy shell five dimensional, with embedded three-dimensional invariant KAM tori. The corresponding PSOS having dimension four is difficult to visualize [3,5–7], and, as in the case of the 2-dof model, the raw data are not expected to provide much structural detail of the chaotic regions. On the contrary, LDs should not have this limitation, being then fully functional to unveil the eventual phase-space structures existing in the chaotic regions of this much more complex case.

In our study, the initial conditions for the trajectories are chosen in the following way. First, we select which fraction of the total energy goes into the C-N motion, and allocate it all in the kinetic energy term, $T_{\text{kin}}^{\text{CN}} = P_r^2/2\mu_2$, since this is the only one able to couple C-N and Li-CN motions. This implies that we take r_e as the initial value for the coordinate r . In our case, we choose $T_{\text{kin}}^{\text{CN}} = 0$, 1000, and 1500 cm^{-1} , presenting the corresponding LD results in the upper, middle, and bottom rows of Fig. 7, respectively. For the remaining $(R, \vartheta, P_R, P_\vartheta)$ variables, we take again random initial conditions in the 2-dof PSOS, as defined in Sec. III.

Figure 7 shows the corresponding LD results for three different values of the total vibrational energy: $E = 3500$, 4000,

and 4500 cm^{-1} in the left, middle, and right columns, respectively. Several comments are in order.

First, a big similarity between the LD corresponding to the 2-dof model of LiCN at the bottom row of Fig. 5, and those for the 3-dof model with an initial null value of $T_{\text{kin}}^{\text{CN}}$ presented in the top row panels of Fig. 7 is found. Obviously, this is not an unexpected result if one takes into account the choice of zero initial kinetic CN energy, and the fact that there exists a good dynamical separation between the C-N and Li-CN motions in our molecule, as demonstrated in Ref. [44]. In any case, this result can be taken as further confirmation of the latter assumption.

Second, more remarkable differences between the 2-dof and the 3-dof descriptions of LiCN are observed when the LDs are computed putting some initial kinetic energy in the CN mode. The corresponding results are found in the middle and bottom rows of Fig. 7. Here, the available phase-space area is smaller than in the previous case (row), due to the motion taking place in the “now hidden” (r, P_r) CN part of the LiCN phase space. Nevertheless, notice how the LDs are still here able to identify the imprints of the invariant manifolds partitioning the phase space in the chaotic regions.

More interestingly, the different columns in Fig. 7 can be interpreted as the (approximate) evolution of the 3-dof invariant manifolds, along with the corresponding trajectories for the full LiCN dynamics actually move. Indeed, due

to Fenichel's theorem, demonstrating the persistence and smoothness of invariant manifolds for flows [45], it is plausible the possibility to construct, from the 2-dof manifolds, the stable and unstable manifolds for the 3-dof coupled model, considering the extra dof and the evolution of a stack of PSOS maps of the 2-dof system calculated at different values of the energy. Also, for the 3-dof Hamiltonian system (1), the resulting invariant manifolds have the correct dimension to exactly divide the phase space completely. A detailed explanation of this way of proceeding can be found in Ref. [46] for a 3-dof extension of the 2-dof system in Ref. [41], where a chaotic scattering problem has been chosen for the calculation. The reason for this is clear, since the existence there of a large portion of the phase space (the asymptotic one) in which the motion is regular (transient chaos) makes the visualization of the problem, i.e., evolution in the stack of reduced dimensionality PSOSs, much easier.

Third, notice that the similarities observed in the manifolds, as pictured by the LD color code, in corresponding (in the energy sense) plots of the previous figures, i.e., between Figs. 7(f) and 5(d), and between Fig. 7(h) with 7(d) and also with Fig. 4(b), are again further indications of the good dynamical separation existing between the C-N and Li-CN motions [44], and also of the resilience of the manifolds of the 2-dof model with respect to the perturbation induced by the (weak) coupling appearing when the CN mode is included.

VI. SUMMARY

In this paper, we have demonstrated the feasibility of using LD to unveil in an easy and effective way the phase-space structures of molecular systems described by realistic potentials. In particular, we have shown the improvement that is obtained with respect to the standard LD definition when p norms are used in it. We have also shown that in this latter case it is very important to make a careful choice of the values of p and the integration time τ , in order to identify clearly the existing homoclinic and heteroclinic intersections, which are

responsible for the intricate dynamics in the chaotic regions of phase space of mixed systems.

Likewise, we have used LDs to explore the phase space of 2-dof and 3-dof vibrational Hamiltonian models for the LiCN molecule, which exhibits a rich dynamical behavior. We have found that LD is an efficient tool to unveil the structure of phase space regardless of the dimensionality of the system, especially in the chaotic area, where other methods find it more difficult to do so. We have also shown—and this is the most important conclusion of our work—that the LD method also works equally well, if not better, in the neighborhood of parabolic points, where the dynamics is nonhyperbolic and marginally stable; something that was not explored in the original works of Mancho *et al.* [16–18], who only considered the effect of hyperbolic points. By comparing the LD obtained in our 2- and 3-dof calculations, we have also ascertained the resilience of the manifolds in the approximated 2-dof model with respect to the introduction of the C-N dof.

To conclude, we give an overview for possible relevant future work. First, the emergence of the invariant structures below and above saddle-node bifurcations should be investigated in more detail using LDs. Second, a detailed procedure for the visualization of the full dimensional dynamics using stacks of (approximate) reduced dimensionality PSOS for the 3-dof model of LiCN should be developed.

ACKNOWLEDGMENTS

This work has been partially supported by the Ministerio de Economía y Competitividad (MINECO) under Contract No. MTM2015-63914-P, ICMAT Severo Ochoa SEV-2015-0554, and from the European Union's Horizon 2020 Research and Innovation Programme under grant agreement No. 734557. F.R. also acknowledges the financial support of the Programa Propio of the Universidad Politécnica de Madrid. We also acknowledge useful discussions with Dr. Mancho, Dr. Balibrea, and Dr. Lopesino on the use of p norms in the definition of LDs.

-
- [1] A. J. Lichtenberg and M. A. Lieberman, *Regular and Chaotic Dynamics* (Springer-Verlag, New York, 2010).
 - [2] J. Guckenheimer and P. Holmes, *Nonlinear Oscillations, Dynamical Systems, and Bifurcations of Vector Fields*, Applied Mathematical Sciences (Springer, New York, 2002).
 - [3] P. A. Patsis and L. Zachilas, *Int. J. Bifurcation Chaos* **04**, 1399 (1994).
 - [4] M. Katsanikas and P. A. Patsis, *Int. J. Bifurcation Chaos* **21**, 467 (2011).
 - [5] S. Lange, M. Richter, F. Onken, A. Bäcker, and R. Ketzmerick, *Chaos* **24**, 024409 (2014).
 - [6] M. Richter, S. Lange, A. Bäcker, and R. Ketzmerick, *Phys. Rev. E* **89**, 022902 (2014).
 - [7] M. Firmbach, S. Lange, R. Ketzmerick, and A. Bäcker, *Phys. Rev. E* **98**, 022214 (2018).
 - [8] P. Cvitanović, R. Artuso, R. Mainieri, G. Tanner, and G. Vattay, *Chaos: Classical and Quantum* (Niels Bohr Institute, Copenhagen, 2016).
 - [9] C. Froeschle, R. Gonczi, and E. Lega, *Planet. Space Sci.* **45**, 881 (1997).
 - [10] C. Froeschlé and E. Lega, *Cel. Mech. Dyn. Astr.* **78**, 167 (2000).
 - [11] R. Barrio, *Chaos, Solitons Fractals* **25**, 711 (2005).
 - [12] C. Skokos, *J. Phys. A* **34**, 10029 (2001).
 - [13] P. Benitez, J. C. Losada, R. M. Benito, and F. Borondo, *Phys. Rev. E* **92**, 042918 (2015).
 - [14] P. M. Cincotta and C. Simó, *Astron. Astrophys. Suppl. Ser.* **147**, 205 (2000).
 - [15] J. A. Jiménez-Madrid and A. M. Mancho, *Chaos* **19**, 013111 (2009).
 - [16] F. Balibrea-Iniesta, C. Lopesino, S. Wiggins, and A. M. Mancho, *Int. J. Bifur. Chaos* **25**, 1550172 (2015).
 - [17] C. Lopesino, F. Balibrea-Iniesta, S. Wiggins, and A. M. Mancho, *Commun. Nonlinear Sci. Num. Simul.* **27**, 40 (2015).
 - [18] C. Lopesino, F. Balibrea-Iniesta, S. Wiggins, and A. M. Mancho, *Int. J. Bifurcation Chaos* **25**, 1550184 (2015).

- [19] F. Balibrea-Iniesta, C. Lopesino, S. Wiggins, and A. M. Mancho, *Int. J. Bifurcation Chaos* **26**, 1630036 (2016).
- [20] M. Feldmaier, A. Junginger, J. Main, G. Wunner, and R. Hernandez, *Chem. Phys. Lett.* **687**, 194 (2017).
- [21] T. Uzer, C. Jaffé, J. Palacián, P. Yanguas, and S. Wiggins, *Nonlinearity* **15**, 957 (2002).
- [22] T. Komatsuzaki and R. S. Berry, *Proc. Natl. Acad. Sci. USA* **98**, 7666 (2001).
- [23] G. T. Craven and R. Hernandez, *Phys. Rev. Lett.* **115**, 148301 (2015).
- [24] G. T. Craven and R. Hernandez, *Phys. Chem. Chem. Phys.* **18**, 4008 (2016).
- [25] A. Junginger, G. T. Craven, T. Bartsch, F. Revuelta, F. Borondo, R. M. Benito, and R. Hernandez, *Phys. Chem. Chem. Phys.* **18**, 30270 (2016).
- [26] A. Junginger and R. Hernandez, *Phys. Chem. Chem. Phys.* **18**, 30282 (2016).
- [27] A. Junginger and R. Hernandez, *J. Phys. Chem. B* **120**, 1720 (2016).
- [28] S. Patra and S. Keshavamurthy, *Phys. Chem. Chem. Phys.* **20**, 4970 (2018).
- [29] R. M. Benito, F. Borondo, J.-H. Kim, B. G. Sumpter, and G. S. Ezra, *Chem. Phys. Lett.* **161**, 60 (1989).
- [30] J. C. Losada, J. M. Estebarez, R. M. Benito, and F. Borondo, *J. Chem. Phys.* **108**, 63 (1998).
- [31] F. Revuelta, T. Bartsch, P. L. Garcia-Muller, R. Hernandez, R. M. Benito, and F. Borondo, *Phys. Rev. E* **93**, 062304 (2016).
- [32] F. Borondo, A. A. Zembekov, and R. M. Benito, *Chem. Phys. Lett.* **246**, 421 (1995).
- [33] F. Borondo, A. A. Zembekov, and R. M. Benito, *J. Chem. Phys.* **105**, 5068 (1996).
- [34] A. A. Zembekov, F. Borondo, and R. M. Benito, *J. Chem. Phys.* **107**, 7934 (1997).
- [35] J. Z. H. Zhang, *Theory and Application of Quantum Molecular Dynamics* (World Scientific, London, 1999).
- [36] R. Essers, J. Tennyson, and P. E. S. Wormer, *Chem. Phys. Lett.* **89**, 223 (1982).
- [37] M. J. Davis, *J. Phys. Chem.* **92**, 3124 (1988).
- [38] A. M. Mancho, S. Wiggins, J. Curbelo, and C. Mendoza, *Commun. Nonlinear Sci. Num. Simul.* **18**, 3530 (2013).
- [39] G. Haller, *Ann. Rev. Fluid Mech.* **47**, 137 (2015).
- [40] C. Lopesino, F. Balibrea-Iniesta, V. J. García-Garrido, S. Wiggins, and A. M. Mancho, *Int. J. Bifurcation Chaos* **27**, 1730001 (2017).
- [41] R. Guantes, F. Borondo, and S. Miret-Artés, *Phys. Rev. E* **56**, 378 (1997).
- [42] F. Revuelta, E. Vergini, R. M. Benito, and F. Borondo, *J. Phys. Chem. A* **120**, 4928 (2016).
- [43] A. Weinstein, *Inv. Math.* **20**, 47 (1973).
- [44] A. Junginger, P. L. Garcia-Muller, F. Borondo, R. M. Benito, and R. Hernandez, *J. Chem. Phys.* **144**, 024104 (2016).
- [45] N. Fenichel, *Indiana Univ. Math. J.* **21**, 193 (1972).
- [46] F. Gonzalez, F. Borondo, and C. Jung (unpublished).